Assessment of the mechanical behaviour of reinforcement bars with localised pitting corrosion by Digital Image Correlation

Engineering Structures 219 (2020) 110936

Contents lists available at ScienceDirect

Engineering Structures

journal homepage: www.elsevier.com/locate/engstruct

Assessment of the mechanical behaviour of reinforcement bars with localised pitting corrosion by Digital Image Correlation

E. Chen[a,*], Carlos G. Berrocal[a,b], Ignasi Fernandez[a], Ingemar Löfgren[a,b], Karin Lundgren[a]

[a] Chalmers University of Technology, Division of Structural Engineering, Göteborg SE-41296, Sweden
[b] Thomas Concrete Group AB, Södra Vägen 28, Göteborg 41254, Sweden

ARTICLE INFO

Keywords:
Pitting corrosion
Mechanical properties
Strain measurement
3D-scanning
Digital Image Correlation

ABSTRACT

Corrosion of reinforcement in concrete impairs the mechanical behaviour of rebars by decreasing their strength and deformation capacity. In this study, uniaxial tensile tests were carried out on 61 rebars taken from 22 pre- and un- cracked reinforced concrete beams subjected to drying and wetting cycles in chloride solution for over three years. A 3D-scanning technique was used to characterise the maximum local corrosion level, μ_{max}, and different pit shape parameters. Digital Image Correlation (DIC) was used to capture the displacement field of the test bars; the engineering strain was measured through the virtual extensometers created in the DIC post-processing software. The proof and ultimate forces showed linear decreasing trends of μ_{max}, while the proof and ultimate strengths (based on the minimum residual cross-sectional area) were not obviously affected by corrosion. The ultimate strain of corroded bars depended on the gauge length due to strain localisation in the pit. Thus, it was emphasised that the ultimate strain may be overestimated if measured based on a short gauge across the pit. It was also observed that when μ_{max} exceeded a critical local corrosion level (μ_{crit} depending on the ratio between the yield and ultimate strengths of the steel), the region outside the pit did not develop yielding. A lower bound of ultimate strain was further derived as a function of the mechanical parameters of uncorroded steel and maximum local corrosion level. This provided a good comparison with the experimental results. Ultimately, a hypothesis for time-dependent assessment of strain capacity is proposed, considering the evolution of corrosion morphology over time.

1. Introduction

Corrosion of steel in concrete is a major cause of impaired safety and durability of infrastructure. As existing structures deteriorate over time due to corrosion, assessing the residual performance of concrete structures accurately becomes imperative, if engineers are to carry out safe, economical maintenance and rehabilitation operations. Corrosion damage in reinforced concrete mainly includes cover cracking, bond degradation of the steel-concrete interface, and undermining the mechanical behaviour of rebars. None of these three issues has been satisfactorily quantified with respect to the corrosion level, even though they have attracted wide interest in recent decades. This may be due to various difficulties including, but not limited to: i) difficulty of quantifying corrosion level accurately and non-destructively; ii) experimental studies usually use higher corrosion rates due to time limitations, altering the corrosion process compared to what occurs in real structures, thus leading to different corrosion morphologies and behaviour of the corrosion products; and iii) corrosion of steel in concrete involves several coupled multi-physical and mechanical processes, which are complex and the interactions of which are not yet fully understood.

In reinforced concrete members, reinforcing steel is the main component carrying tensile stress. Understanding the mechanical properties of corroded rebars is essential to the development of reliable assessment models for corroded structures. The effects of corrosion on the mechanical properties of reinforcing bars have primarily been investigated through experimental testing. Empirical relationships which fit the mechanical properties to various corrosion features have been suggested, see [1–14] for example. Although existing research indicates that the load capacity and ductility of steel bars are reduced with increasing corrosion level, the empirical relationships derived for the mechanical parameters (as a function of corrosion level) vary significantly between different studies and, in some cases, even contradict each other. This is most likely attributable to variations in the type of corrosion condition and type of steel, plus the different evaluation methods used in quantifying corrosion levels and mechanical

* Corresponding author.
E-mail address: teresa.chen@chalmers.se (E. Chen).

https://doi.org/10.1016/j.engstruct.2020.110936
Received 19 March 2020; Received in revised form 25 May 2020; Accepted 4 June 2020
Available online 15 June 2020

Nomenclature

A	cross-sectional area of a steel bar
A_{min}	minimum cross-sectional area along a bar
$A_{0,min}$	original area of the cross-section with the minimum remaining area
A_0	nominal cross-sectional area of uncorroded bars
E_0	Young's modulus of uncorroded bars
P	strain-hardening power of uncorroded bars
E_{sh0}	strain-hardening modulus of uncorroded bars, i.e. tangent slope at ε_{sh0}
F	tensile force
F_{corr}	proof or ultimate force of corroded bars, either $F_{t0.5}$ or F_u
F_0	yield or ultimate force of uncorroded bars, either F_{y0} or F_{u0}
$F_{t0.5}$	proof force, defined as the force at $\varepsilon_{t0.5}$ based on 50 mm extensometer
F_u	ultimate force
F_y	yield force
L_0	bar length
$f_{t0.5}$	proof strength, defined as the stress at $\varepsilon_{t0.5}$ based on 50 mm extensometer
f_u	ultimate strength
f_{u0}	ultimate strength of uncorroded bars
f_y	yield strength
f_{y0}	yield strength of uncorroded bars
l_g	extensometer gauge length
l_p	pit length
w_p	pit width at the minimum cross-section
x_p	pit depth at the minimum cross-section
ε_{sh0}	strain at the onset of hardening of uncorroded bars
$\varepsilon_{t0.5}$	proof strain when the total extension is 0.5%, based on the 50 mm extensometer
ε_u	ultimate strain, defined as the strain at the ultimate force
ε_{u0}	ultimate strain of uncorroded bars
$\varepsilon_u(x)$	local strain at ultimate strain at x position
ε_{y0}	strain at the onset of yielding of uncorroded bars
ε^{25}	strain measured from 25 mm extensometer across the failure zone
ε^{50}	strain measured from 50 mm extensometer across the failure zone
ε^{75}	strain measured from 75 mm extensometer across the failure zone
ε^{5_out}	strain measured from 5 mm extensometer outside the failure zone
ε^{10_out}	strain measured from 10 mm extensometer outside the failure zone
ε^{25_out}	strain measured from 25 mm extensometer outside the failure zone
ε^{380}	strain measured from the total elongation of tested bars
ε_u^{25}	ultimate strain measured from 25 mm extensometer across the failure zone
ε_u^{50}	ultimate strain measured from 50 mm extensometer across the failure zone
ε_u^{75}	ultimate strain measured from 75 mm extensometer across the failure zone
$\varepsilon_u^{5\_out}$	ultimate strain measured from 5 mm extensometer outside the failure zone
$\varepsilon_u^{10\_out}$	ultimate strain measured from 10 mm extensometer outside the failure zone
$\varepsilon_u^{25\_out}$	ultimate strain measured from 25 mm extensometer outside the failure zone
ε_u^{380}	ultimate strain measured from the total elongation of tested bars
$\varepsilon_u^{l_g}$	ultimate strain over the gauge length l_g
ε_u^{out}	ultimate strain outside the pit over any gauge length greater than one rib spacing
α	empirical coefficient to indicate the degradation rate of the force with μ_{max}
σ	tensile stress in steel bars, which is calculated based on A_{min}
δ_u	total displacement at the ultimate force
μ_{weight}	corrosion level from the weight loss method
μ	corrosion level
μ_{max}	maximum local corrosion level along a bar, defined as the maximum cross-sectional area loss percentage
μ_{crit}	critical local corrosion level, above which no yielding occurs outside the pit

properties, see [1,2,4,6,11,14] for example.

The specimens examined in the literature include bare bars and bars extracted from concrete. Bar corrosion was produced using several different methods: applying impressed current [1,2,6,7,12], exposure to chloride spray in the laboratory [4,5,10,11], simulating corrosion damage with machined defects [1,2,11], and natural corrosion in real structures [13,14]. From previous studies, the reduction in both yielding force and maximum force displayed a linear trend with increasing corrosion level. Moreover, some studies [6,14] indicated that the decreasing slope is strongly dependent on how the corrosion level is determined: average cross-sectional area loss from the total weight loss or maximum cross-sectional area loss from advanced image techniques such as 3D-scanning. The type of steel may also influence the results, as mentioned in [14]. For steel with heterogeneous microstructure and mechanical properties throughout the bar cross-section, such as TEMPCORE steel [15], the relative contribution of the area loss in each layer to the strength loss may differ.

For the stresses at yielding force and maximum force, when they were calculated as the ratio between the force and the nominal cross-sectional area or average remaining cross-sectional area, a decreasing trend with increasing average corrosion level was observed [1,5–7,14]. When the minimum remaining cross-sectional area was used to calculate the stress, it was observed [5,6,14] that the stresses at yielding and at maximum force were not significantly affected by corrosion. They even exhibited a slightly increasing trend at higher corrosion levels.

Regarding the deformation and ductility behaviour of corroded rebars, it has been widely reported that, compared to the loss of load capacity, the ultimate strain decreased more markedly with increasing corrosion levels [2,4–6,10,11,14]. It should be noted that, in most studies, "ultimate strain" referred to the strain at maximum force, whereas a few used it to mean the strain at failure. Throughout this paper, "ultimate strain" is defined as the strain at maximum force. Many studies [5,6,10,11] have proposed an exponential decaying function for the ultimate strain versus the corrosion level, with different studies suggesting different empirical coefficients. One study [11] demonstrated that different corrosion morphologies led to significantly different decaying factors of the ultimate strain in terms of corrosion level, by comparing three groups of specimens with artificial notches of various shapes. Furthermore, in the tensile test, it is evident that different extensometer gauge lengths have been chosen by different researchers to measure the ultimate strain, such as 50 mm [7,14], 100 mm [4], 200 mm [1], five times the bar diameter [13], ten times the bar diameter [11], and the total length of tested bars [6]. A previous study [1] speculated that the gauge length may influence the strain results, as the local yielding elongation over the failure zone may be very different compared to the total elongation of corroded rebars. However, to the authors' knowledge, there have been no prior studies specifically investigating the effect of gauge length on the deformation

capacity of corroded rebars.

Most literature studied bars corroded by impressed current [1,2,6,7,12], which induced corrosion throughout the length of the bar and a mixed morphology of general and pitting corrosion. A few studies investigated bars taken from real structures, which had naturally corroded for decades [13,14]. They simultaneously exhibited noticeable uniform corrosion and pit attacks, representing the advanced stages of chloride-induced corrosion [14]. The corrosion morphology of isolated localised pits formed under natural corrosion conditions has rarely been studied. However, this type of corrosion is common in practical reinforced concrete structures [16], particularly in the early stages of corrosion, which is caused by pre-existing cracks in concrete. Furthermore, localised pitting is a more dangerous corrosion condition compared to general corrosion and extensive pitting corrosion (in other words, when pitting corrosion spreads over the whole bar surface). This is because there may be a lack of warning, in the form of visible corrosion-induced cover cracking [16].

This study tested corroded bars extracted from pre- and un- cracked reinforced concrete beams which had been subjected to cyclic wet-drying exposure to chloride solution for over three years. The bars showed isolated corrosion pits, with negligible superficial corrosion surrounding the pits. The purpose of this study was to quantify the strength and strain capacity of TEMPCORE steel rebars with localised pitting corrosion as a function of corrosion level. A 3D-scanning technique was used to characterise the pit morphology accurately, while Digital Image Correlation (DIC) was used to measure the deformation of the corroded bars during tensile testing. The local strain distribution and ultimate strain (based on different virtual extensometers created in the DIC post-processing software) were evaluated using a real-time displacement field along the bar and within the measuring volume of the DIC cameras. Based on the DIC findings, an analytical model and a semi-analytical model were proposed to calculate the ultimate strain for any gauge length greater than the pit length. Subsequently, the experimental results of the ultimate strain were compared to other studies

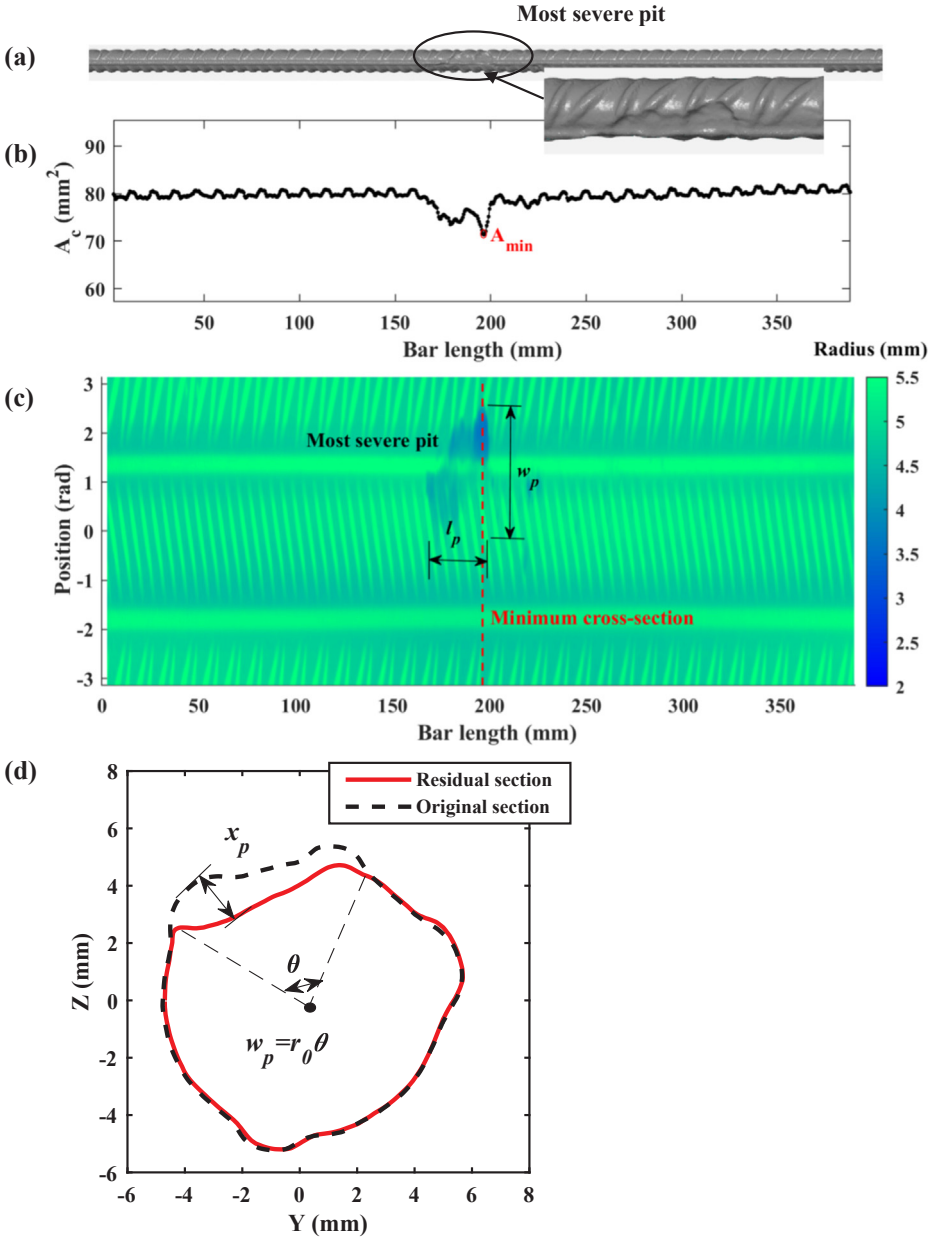

Fig. 1. Example illustrating corrosion evaluation from 3D-scanning: (a) reconstructed bar surface from 3D-scanning; (b) longitudinal variation of cross-sectional area along the scanned length; (c) 2D plot of the bar surface with colour scale showing the magnitude of radius; (d) residual and original cross-sectional appearance at the minimum cross-section.

investigating bars with different corrosion morphologies and using different strain measurement lengths. Finally, the degradation of strain capacity with corrosion time was discussed, relative to the evolution of corrosion morphology over time.

2. Experimental description

2.1. Specimens

Hot-rolled ribbed TEMPCORE steel reinforcement bars were used in this study. The steel class was normal-ductility B500B, as defined in Appendix C of Eurocode 2 [17]. The bars had a nominal diameter of 10 mm. They were extracted from 22 reinforced concrete beams (1100 × 180 × 100 mm), with 18 beams pre-cracked to a crack width of either 0.1 or 0.4 mm under a three-point bending configuration. The remaining four were uncracked. After the initial pre-cracking, all beams were subjected to cyclic wet-drying exposure to chloride solution (of 16.5% NaCl concentration) for three years and stored in the laboratory for an additional one or two years before the bars were extracted. Further details of the beams' preparation and corrosion environment can be found in [18].

After the rebars were extracted from the beams, they were cleaned by sand-blasting, according to [19]. They were then cut with an electrical rebar cutter to obtain 500 mm segments, with the most severe pitting located near the centre. Where more than two pits of similar severity were found in relatively close proximity, the segment length was extended to 550 mm, to incorporate both pits within the same specimen. A total of 61 bars were tested, including five uncorroded bars.

2.2. Corrosion level evaluation with 3D-scanning

Traditionally, the corrosion level is determined by the gravimetric weight loss method. The gravimetric weight loss of all specimens (i.e. cut bar segments) in this study was found to be less than 3.5%. However, this method is not considered appropriate for evaluating pitting corrosion, as the weight loss in the pit was very small compared to the weight of the whole bar. Instead, the local corrosion level was evaluated by 3D-scanning of the steel bar surface. A portable laser scanner (Handy Scan 700TM from Creaform) was used, with an accuracy of up to 20 μm and a maximum spatial resolution of 0.05 mm in the resulting point cloud. Based on the method developed in [20], the point cloud constituting the surface mesh was imported into MATLAB [21] to evaluate the cross-sectional area along the bar and the geometrical parameters of the pit. The 3D surface mesh of one bar is shown in Fig. 1a, with details of the most severe pit amplified.

Fig. 1b shows the cross-sectional area A along the axis direction for one bar. The periodic variation in cross-sectional area of the plot is due to the presence of ribs on the bar surface. The local corrosion level is defined as the area loss percentage at each cross-section. According to Eq. (1), the maximum local corrosion level, μ_{max}, is determined at the section with minimum remaining cross-sectional area, A_{min}:

$$\mu_{max} = \frac{A_{0,min} - A_{min}}{A_{0,min}} \tag{1}$$

where $A_{0,min}$ is the original cross-sectional area of the section with the minimum remaining cross-sectional area. The original uncorroded cross-section was found using an iterative process developed in [22] by comparing the healthy part of the corroded section with each section in the uncorroded segment covering a complete interval of transverse rib variation. The 3D coordinates of points composing the bar surface are shown in a 2D plot, with the colour representing the radius of every point, as in Fig. 1c. The appearance of the minimum cross-section and its original uncorroded section are shown in Fig. 1d. The pit length l_p was the length of the corrosion pit along the bar axis, while the pit depth x_p and pit width w_p were determined at the minimum cross-section, as shown in Fig. 1d.

2.3. Tensile test procedure

Monotonical uniaxial tensile tests were conducted on the steel bars, using an MTS universal testing machine and according to BS EN ISO standard [23]. At each bar end, a 60 mm length was clamped in the grip zones. Hence, the tested length subjected to tension was 380 mm for the 500 mm bars and 430 mm for two 550 mm bars. The loading was applied under displacement control, with a 0.5 mm/min rate in the elastic stage and 2 mm/min afterwards. The force applied and total machine displacement were recorded.

2.3.1. DIC system

The DIC measurements conducted in this study were carried out using the ARAMIS Adjustable camera system, equipped with 12Mp sensors, dual-LED lighting and ARAMIS Professional software. The camera resolution in this system is 4096 × 3000 pixels and the frame rate goes from 25 to 100 frames per seconds (fps). The measurement area ranges from 20 × 15 mm^2 to 5000 × 4000 mm^2.

Before testing, a stochastic speckle pattern was created on the bar surfaces by alternate spraying with black and white paint [24]. Fig. 2 shows the painted bars and Fig. 3 the experimental setup with the DIC equipment. The camera lenses were 75 mm and the system was initially calibrated to calculate the position and orientation of each camera. The camera rig was then adjusted horizontally and vertically, without changing the relative positions of the cameras. This was done to include the most severe pit in the measurement volume and allow the failure zone to be captured. Based on the quality of the speckle patterns generated on the bar surfaces, the measurement volume was set to 100 × 75 × 55 mm to ensure good measurement resolution, while the facet size was set to 15 × 13 pixels. The acquisition rate was set to 5 Hz. To reduce the file size of the results, only every twentieth image was stored (or every four seconds) by setting the frequency divider to 20. A ring buffer was set to ensure storage of the last 150 images before failure (equivalent to the last 30 s of the test). Moreover, the data logger of the MTS machine was connected to the ARAMIS software, to synchronise data measurements of the applied force and total displacement of the testing machine.

2.3.2. Post-processing of the DIC measurement

The results were post-processed in GOM Correlate Professional software [25]. The engineering strain was computed for this study; this

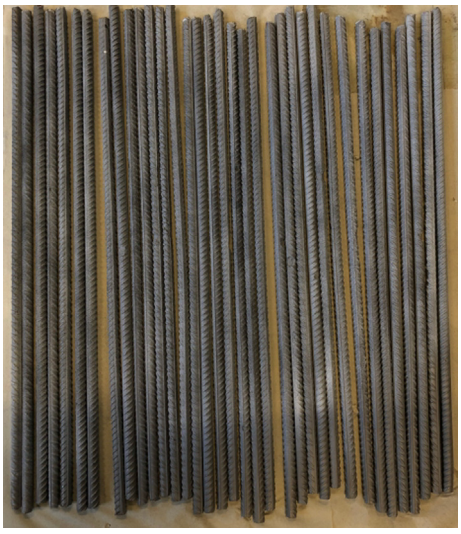

Fig. 2. Steel bars with stochastic paint.

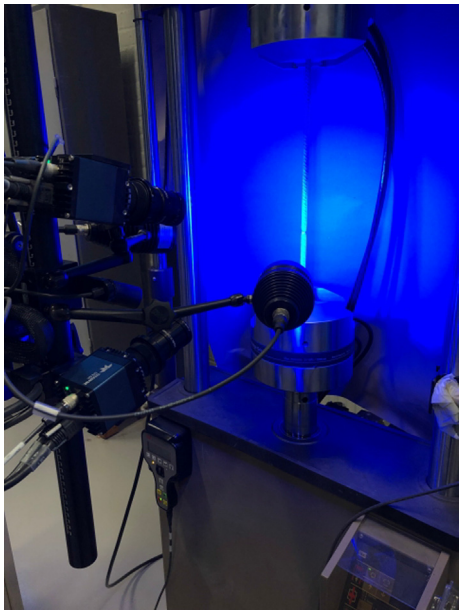

Fig. 3. DIC setup for the tensile test.

is defined as the change of a reference length relative to its original length. The reference length for the strain calculations was defined by constructing virtual extensometers, using a built-in feature of the GOM software. To compare the strain at different regions of the corroded bars, a total of six virtual extensometers were created along the bar axis; three across the failure zone with lengths of 25, 50 and 75 mm, and three outside the failure zone with lengths of 5, 10 and 25 mm (see Fig. 4). The constraints of the measuring volume (and elongation of the bar itself) limited the maximum length of the virtual extensometer to 75 mm.

In the following sections, to avoid confusion when describing the strain values, the gauge length of the extensometer will be indicated, when necessary, as a superscript to the strain symbol ε. For example, ε^{50} represents the strain measured by the 50 mm gauge across the failure zone, and ε^{25_out} the 25 mm gauge outside it. Also, to validate the DIC measurements, a traditional extensometer was mounted on three specimens, with a gauge length of 50 mm. Fig. 5 shows the force-strain curve of one of the bars, which exhibits excellent agreement between both measurements.

2.3.3. Definitions of the mechanical parameters of bars

First, the terminology for the mechanical parameters studied in this paper was defined. The maximum force is termed “ultimate force”. Correspondingly, the stress at maximum force is defined as “ultimate strength”. The stress of corroded bars is calculated from the minimum cross-sectional area, as in Eq. (2):

$$\sigma = \frac{F}{A_{min}} \tag{2}$$

where σ is the stress and F is the force.

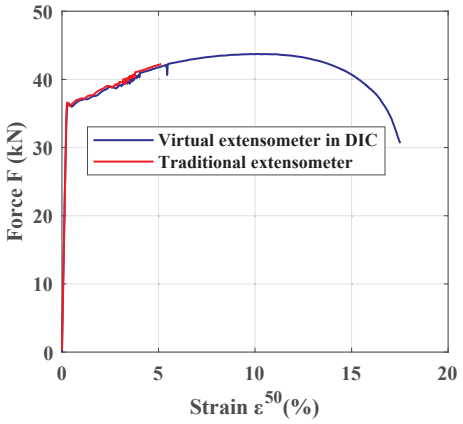

Fig. 5. Comparison of force-strain curves from the DIC and traditional extensometer.

For steel with an obvious yield plateau, as illustrated in Fig. 6a, the yielding force F_y and yield strength f_y can be defined according to the BS EN ISO standard [23]. However, for steel without a yield plateau, yield strength is replaced by proof strength, which is defined as the stress at a prescribed plastic or total extension [23]. Even though the uncorroded steel bars used in this study presented a distinct yield plateau, the pronounced effect of corrosion on the force-strain diagram made it difficult to accurately determine the force and stress upon yielding for corroded bars. Consequently, in this study, a total extension of 0.5% (based on a 50 mm extensometer) was defined as the proof strain. This is noted as $\varepsilon_{t0.5}$ and was measured so as to obtain the proof force (defined as the force at proof strain, noted as $F_{t0.5}$) and proof strength (noted as $f_{t0.5}$) of all the corroded bars, see Fig. 6b. It should be noted that for uncorroded bars and lightly corroded bars exhibiting the yield plateau, the proof strength $f_{t0.5}$ is nearly the same as the yield strength. This is because the proof strain of 0.5% is within the yield plateau, where the stress is almost constant.

The mechanical characteristics of the uncorroded bars were calculated by averaging the results of five uncorroded bars. From the average values of yielding force F_{y0} and ultimate force F_{u0}, and the nominal area of the uncorroded bars (A_0 = 78.54 mm^2), the yield strength f_{y0} and ultimate strength f_{u0} were calculated as 532 MPa and 613 MPa. The strain at onset of yielding and hardening of uncorroded bars was ε_{y0} = 0.27% and ε_{sh0} = 2.7% respectively, while the strain at ultimate force ε_{u0} was 10.79%.

3. Results

This section presents the results of corrosion characteristics and mechanical parameters. All the data appears in Tables 1 and 2.

3.1. Corrosion morphology

Along the rebar length, corrosion pits were generally found near the flexural cracks. In uncracked beams, numerous tiny pits were also formed on the surface of the bars. The observed shape of the pits was

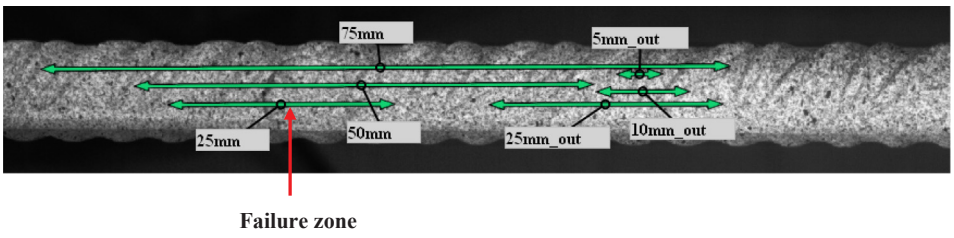

Fig. 4. Extensometers defined in the DIC post-processing software.

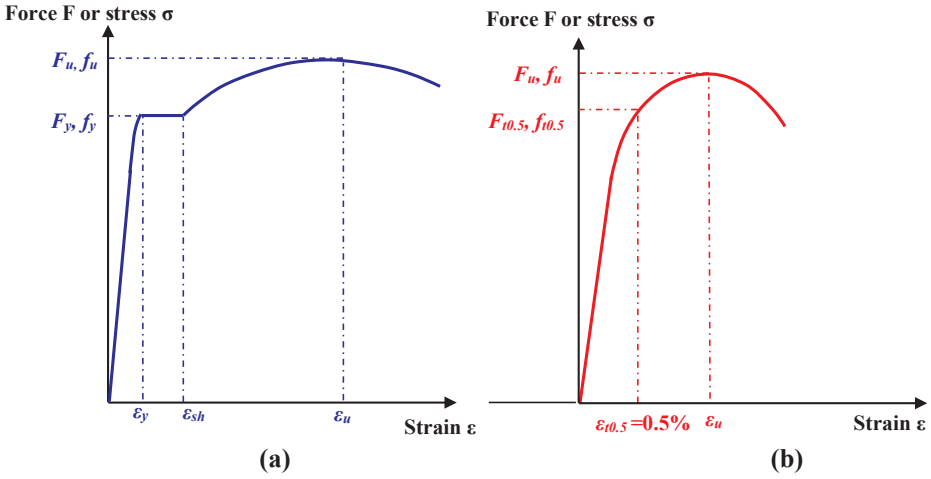

Fig. 6. Definition of main mechanical parameters according to the standard [23]: (a) for steel with obvious yield plateau; (b) for steel without yield plateau.

mainly elliptical, while some pits exhibited extended corrosion next to the elliptical cavity, probably caused by longitudinal corrosion-induced cracks along the beams. However, the pit length did not exceed 100 mm in any of the studied rebars. Surrounding the pit, the surface of the bars showed almost no corrosion. Unlike bars subjected to impressed current or natural corrosion for decades, the corrosion of the bars in this study was particularly localised. This may relate to the corrosion condition in the present study; the high chloride concentration may have caused a very high local corrosion rate in the pits. Moreover, during the relatively short exposure time (three years), the corrosion process near the flexural cracks had not been significantly influenced by corrosion-induced (longitudinal) cracks, as they had not developed along the whole beam length. Similar type of corrosion may be formed in practice due to the undesirable pre-existing cracks and/or highly non-uniform exposure conditions between different regions of the structures. The correlation between concrete cracks and corrosion characteristics of the beams in this study can be found in a previous study of the authors [26].

The relationships between the main pit morphology parameters shown in Table 1 were examined. Bars with higher maximum local corrosion level usually exhibited greater pit depth and pit width too, however, the correlations between maximum local corrosion level and pit depth or pit width were generally poor. It was found that the product of the pit depth and pit width had a clear linear relationship to the maximum local corrosion level. Therefore, the maximum local corrosion level can actually reflect the combined feature of pit depth and pit width for the specimens in this study. The pit length, however, has no obvious correlation with the maximum local corrosion level or other pit geometries. In the following, the maximum local corrosion level was used as the main parameter for correlating with the mechanical properties, while the influence of pit length was examined as well on the strain properties.

3.2. Force-strain curves

The force-strain curves of all the bars are shown in Fig. 7. The strain in those curves was based on the 50 mm extensometer, which is five times the nominal diameter; a length specified in the BS EN ISO standard [23]. The colour of each curve, changing from dark blue to bright red, represents the maximum local corrosion level, μ_{max}, ranging from 0 to 35%. As clearly observed in Fig. 7, the shape of the force-strain curve is deeply affected by the maximum local corrosion level. Uncorroded steel bars exhibit a distinct yield plateau before strain-hardening. However, when μ_{max} is greater than about 10%, the yield plateau becomes indiscernible and the strain-hardening stage is simultaneously reduced, leading to a brittle failure at higher corrosion levels.

3.3. Strength versus maximum local corrosion level

The relationships of the proof and ultimate forces ($F_{t0.5}$ and F_u) to the maximum local corrosion level are shown in Fig. 8, in which a clear, decreasing linear trend is observed. These relationships were determined using the following linear expression, which is commonly used in the literature [14]:

$$F_{corr} = F_0(1 - \alpha\mu) \tag{3}$$

where F_{corr} is the proof or ultimate force of corroded bars, either $F_{t0.5}$ or F_u, F_0 is the yielding or ultimate force of uncorroded bars, either F_{y0} or F_{u0}, μ is the corrosion level (either average corrosion level or maximum local corrosion level) and α is the empirical coefficient indicating the degradation rate of the force loss (ranging from 1 to 3 in most previous studies). The maximum local corrosion level μ_{max} was used in the above expression. From the linear regression, the α coefficients were found to be 1.05 and 0.87 for the proof and ultimate forces respectively. These results indicate that the proof force decreases at a similar rate to that of the maximum cross-sectional area loss, while the degradation rate of the ultimate force is slightly less than the maximum cross-sectional area loss.

The proof and ultimate strengths ($f_{t0.5}$ and f_u) were obtained using Eq. (2). Their relationships to the maximum local corrosion level are shown in Fig. 8b. There is no clearly observed dependence of strength on maximum local corrosion level. Considering the natural scatter of the strength of uncorroded bars, it may be inferred that the strength was almost unaltered. Indeed, a small increasing tendency is observed at higher corrosion levels, similar to the results reported in [5,6,14]. One possible explanation for this behaviour was given in [14], where it was hypothesised that bars with higher corrosion levels present less necking and that, consequently, the apparent stress (measured from the minimum cross-sectional area before loading) is closer to the true stress than for uncorroded steel bars.

Another possible reason may be related to the properties of TEMPCORE steel, which has a higher-strength martensitic crown and a lower-strength ferrite core. Although uniformly reducing the steel cross-section from the out-layer towards the inner core can result in a gradual loss of strength (as shown in [27]), this may not be the case for pitting corrosion. This is because, in bars with localised area loss at higher corrosion levels, the relative percentage of inner core area loss may increase. However, this explanation needs further verification through the microstructure characterisation of the TEMPCORE steel cross-section.

Table 1
Pit characteristics and ultimate strain.

Bar No.	μ_{max}(%)	A_{min} (mm^2)	l_p (mm)	w_p (mm)	x_p (mm)	ε_u^{380} (%)	ε_u^{50} (%)
104	0.00	78.57	0.00	0.00	0.00	11.67	N/A
25	0.00	79.71	0.00	0.00	0.00	11.78	N/A
44	0.00	79.67	0.00	0.00	0.00	10.11	N/A
50	0.00	78.26	0.00	0.00	0.00	12.62	N/A
51	0.00	79.13	0.00	0.00	0.00	12.50	12.57
160	1.56	78.44	1.56	1.56	0.31	11.26	11.88
98	2.50	77.89	2.50	1.67	0.49	10.72	12.47
43	3.11	74.85	2.78	3.08	0.69	10.29	11.64
49	3.26	77.21	3.89	2.67	0.85	10.30	12.75
103	3.53	78.56	2.21	2.25	0.90	9.26	10.09
36	3.54	76.96	2.79	2.58	0.84	9.32	N/A
27	4.05	77.89	3.01	2.09	0.99	9.94	11.60
26	4.20	77.06	4.98	4.92	0.77	10.79	11.83
105	4.36	74.67	4.17	3.33	0.97	7.95	9.31
45	4.53	74.81	4.17	3.92	0.83	9.71	N/A
171	5.01	75.18	8.34	4.92	1.26	6.87	8.84
169	5.03	77.32	2.51	2.46	0.92	9.47	10.91
35	5.36	73.96	4.16	3.67	0.97	7.82	9.30
109	5.77	74.34	2.76	3.42	0.79	7.55	9.72
72	5.83	74.84	7.49	4.92	1.30	8.17	10.04
3	5.88	73.85	3.89	2.42	0.92	9.67	10.08
131	6.30	73.39	48.04	7.83	0.72	7.95	10.95
132	7.40	73.41	6.94	6.00	1.48	6.78	8.83
14	7.47	73.42	12.88	4.40	1.63	5.76	7.89
161	7.66	75.01	23.12	5.55	1.30	6.49	9.03
71	8.33	71.56	5.81	4.58	1.40	6.61	8.54
99	8.55	73.09	4.44	4.58	1.54	6.55	8.66
101	8.67	73.07	5.78	3.46	1.42	6.84	11.17
58	8.68	71.52	44.70	9.75	0.99	5.46	8.98
60	9.15	71.99	31.39	6.75	1.35	5.54	10.13
170	9.89	72.32	6.39	6.38	2.01	5.35	7.65
159	9.94	71.38	32.01	6.90	1.74	4.73	8.91
23	10.05	72.39	34.17	9.81	1.56	4.32	8.42
24	10.37	72.90	65.27	9.25	1.55	4.72	8.74
164	11.17	69.98	6.03	10.50	1.18	4.46	6.32
40	11.23	71.64	30.47	10.00	1.62	4.98	10.48
34	11.79	70.66	71.33	6.10	2.03	5.70	8.78
15	12.01	69.88	55.79	9.75	1.64	4.74	8.49
100	12.58	69.08	20.98	6.78	1.85	4.26	7.32
158	12.82	71.17	27.01	6.65	1.93	4.49	8.02
2	12.82	69.81	58.35	9.58	1.64	4.41	8.44
157	13.83	68.65	13.15	12.75	1.44	3.26	6.14
22	14.19	69.29	18.60	12.88	2.12	1.21	6.21
162	14.86	68.67	45.03	10.42	1.59	3.80	7.45
1	15.16	66.74	36.65	12.55	1.53	4.44	9.19
165	15.29	69.27	14.33	7.81	2.11	4.14	6.80
163	15.39	68.39	42.49	13.37	1.70	1.33	7.18
110	15.71	66.13	10.00	8.42	2.07	3.24	5.60
42	15.85	65.89	25.32	15.49	1.66	1.19	5.35
130	17.18	65.93	93.58	12.55	1.69	2.47	9.24
174	17.40	65.73	39.75	9.47	3.42	1.13	5.79
13	18.63	62.72	12.22	8.42	2.65	2.84	5.76
111	19.34	62.57	34.16	13.67	1.82	1.08	6.63
67	20.11	63.20	46.12	13.85	2.35	1.19	5.69
68	20.36	61.43	62.79	9.00	2.70	1.27	5.69
97	22.55	61.35	40.26	13.00	2.60	1.01	5.02
172	23.34	61.90	43.13	8.20	3.08	1.19	4.45
70	26.03	58.95	51.43	11.25	3.36	1.04	4.63
62	26.39	57.23	8.33	23.92	1.77	0.63	2.53
61	32.68	51.85	11.39	16.17	2.30	0.58	2.25
63	33.65	51.84	12.78	21.67	2.26	0.61	2.64

3.4. Strain properties

3.4.1. Local strain distribution and evolution

The axial strain, computed as the maximum principal strain in the local coordinate, was examined at every point on the bar surface within the measuring volume captured using DIC. To illustrate how corrosion affected the axial strain distribution of bars and its evolution during the tensile test, seven different maximum local corrosion levels, including the uncorroded case, were selected for comparison: 0%, 5.4%, 11.2%, 15.7%, 20.4%, 26.0% and 32.7%. Fig. 9 shows the axial strain field at proof strain ($\varepsilon_{t0.5}$) and ultimate strain (ε_u), for each corrosion level. To facilitate comparison of the results between the seven bars, the upper and lower limits of the legend were kept constant. Histograms showing the distribution of local strain values along the bar were also displayed next to the legends.

Further, the local strain values along one longitudinal section (at proof and ultimate strains) were obtained for all bars shown in Fig. 9. These are plotted in Fig. 10, where the longitudinal strain distribution at different corrosion levels may be compared quantitatively. Additionally, the local strain distribution of the uncorroded bar at two loading stages additional to $\varepsilon_{t0.5}$ and ε_u (namely $\varepsilon_1 < \varepsilon_{t0.5}$ and $\varepsilon_2 > \varepsilon_u$) is shown in Fig. 11. At ε_1, the strain distribution was uniform along the whole bar length; at $\varepsilon_{t0.5}$, yielding developed only within a limited region in the rebar. Subsequently, yielding and hardening spread along the whole bar without strain localisation until $\varepsilon_u$was reached. This implies that for the uncorroded bar, the ultimate strain (measured by extensometer) would be independent of gauge length and position, provided the gauge length was greater than the distance between two consecutive ribs. Finally, at ε_2 (a stage following necking of the uncorroded bar), strain localisation in the necking zone became apparent, as shown in Fig. 11.

From Fig. 10a, at the proof strain, the maximum value of the local strain for all the corroded bars was much higher than that of the uncorroded bar. This indicates very early strain localisation in corroded bars, even when the maximum local corrosion level was only 5.4%. At ultimate strain, the maximum local strain was also greater in corroded bars than in the uncorroded bar. This was because strain localisation for the uncorroded bar did not occur until after ultimate strain. At ultimate strain, it displayed a rather uniform strain distribution of about 10% (after averaging the local effects caused by the ribs). Conversely, corroded bars displayed much lower local strain values outside the pit; a phenomenon which becomes more pronounced as the maximum local corrosion level increases.

3.4.2. Ultimate strain ε_u^{50} versus μ_{max} and influence of pit length

The ultimate strain ε_u^{50} (normalised by the average value of uncorroded steel bars ε_{u0}) versus the maximum local corrosion level μ_{max} is plotted in Fig. 12. There is a clear decreasing trend, yet the scatter is large; at similar maximum local corrosion levels, the measured strain differed by a factor of almost 2 for some rebars. As the pit shape in different bars was diverse in numerous ways, the scatter is not surprising when only the maximum local corrosion level was plotted against the ultimate strain. The other pit geometry parameters should also influence the ultimate strain. Since the pits introduce a sudden change in geometry that disrupts the strain field in a bar, it was hypothesised that pit length may play an important role in strain localisation. Thus, pit length was introduced in Fig. 12 to examine its influence and is depicted by marker colour. It can be observed that, at similar maximum local corrosion levels, most of the points with longer pit length have greater strain than shorter pits represented by the blue and green points.

The local strain distribution of bars with similar maximum local corrosion levels but a major difference in pit length was examined in the four bars (labelled in Fig. 12 by their respective numbers). Fig. 13 shows their local strain distribution at ultimate strain, plus their corrosion morphologies. In bars with longer pits, strain localisation occurred across a greater portion of the bar length. As a result, the strain over a given gauge length was greater (almost one time larger) for the bar with much longer pit length than the bar with shorter pit length although their maximum local corrosion level was close. Therefore, besides the maximum local corrosion level, the pit length also plays an important role in the ultimate strain of corroded bars.

Table 2
Tensile test results.

bar No.	L_0 (mm)	μ_{max}(%)	F_u (kN)	$F_{t0.5}$ (kN)	δ_u (mm)	ε_u^{380} (%)	ε_u^{25} (%)	ε_u^{50} (%)	ε_u^{75} (%)	$\varepsilon_u^{5\_out}$ (%)	$\varepsilon_u^{10\_out}$ (%)	$\varepsilon_u^{25\_out}$ (%)
104	500	0.00	46.76	40.42	44.34	11.67	N/A	N/A	N/A	12.15	10.74	9.81
25	500	0.00	52.02	44.94	44.76	11.78	N/A	N/A	N/A	8.79	10.37	10.24
44	500	0.00	48.82	42.79	38.42	10.11	N/A	N/A	N/A	8.89	9.36	9.28
50	500	0.00	45.45	39.06	47.96	12.62	N/A	N/A	N/A	9.46	9.96	10.69
51	500	0.00	47.80	41.57	47.49	12.50	12.86	12.57	N/A	11.39	10.50	11.61
160	500	1.56	46.88	40.10	42.77	11.26	12.55	11.88	11.20	9.24	10.02	10.57
98	500	2.50	50.53	43.33	40.72	10.72	13.71	12.47	N/A	10.07	10.31	10.57
43	500	3.11	48.27	40.19	39.09	10.29	12.74	11.64	11.12	11.46	10.27	10.34
49	500	3.26	47.30	40.79	39.14	10.30	12.65	12.75	11.41	8.72	9.64	10.14
103	500	3.53	47.85	40.09	35.19	9.26	12.11	10.09	9.34	7.25	7.72	7.78
36	500	3.54	47.84	41.22	35.41	9.32	N/A	N/A	N/A	8.83	9.07	9.46
27	500	4.05	48.72	40.53	37.78	9.94	13.42	11.60	10.74	10.36	8.69	9.61
26	500	4.20	47.44	40.86	41.00	10.79	13.57	11.83	11.47	12.68	9.88	10.38
105	500	4.36	46.96	39.72	30.20	7.95	11.04	9.31	8.15	5.82	6.76	6.67
45	500	4.53	48.43	41.41	36.90	9.71	N/A	N/A	N/A	7.15	6.77	7.45
171	500	5.01	47.02	39.16	26.09	6.87	11.19	8.84	7.77	5.81	5.44	5.57
169	500	5.03	49.47	42.65	35.99	9.47	12.11	10.91	N/A	8.23	8.41	8.09
35	500	5.36	46.02	38.66	29.72	7.82	11.66	9.30	8.13	6.03	5.85	6.04
109	500	5.77	47.13	38.71	28.70	7.55	11.97	9.72	7.87	5.76	6.41	6.64
72	500	5.83	47.97	39.68	31.04	8.17	11.16	10.04	8.81	6.44	6.51	6.80
3	500	5.88	48.52	40.38	36.75	9.67	12.55	10.08	9.57	7.86	7.10	6.70
131	500	6.30	46.85	38.64	30.22	7.95	13.91	10.95	9.23	7.45	6.94	6.81
132	500	7.40	46.55	38.78	25.76	6.78	10.29	8.83	8.01	6.12	5.73	6.00
14	500	7.47	46.39	38.94	21.90	5.76	10.19	7.89	6.96	4.52	4.92	5.36
161	500	7.66	46.12	38.20	24.65	6.49	10.77	9.03	8.55	4.57	6.50	8.31
71	500	8.33	47.72	39.41	25.11	6.61	10.63	8.54	7.46	5.37	5.67	6.13
99	500	8.55	45.83	38.16	24.91	6.55	10.77	8.66	7.32	5.15	5.65	5.24
101	500	8.67	46.55	39.52	25.98	6.84	12.68	11.17	8.96	6.24	6.35	7.89
58	500	8.68	44.26	36.63	20.75	5.46	12.17	8.98	7.16	4.30	3.21	4.22
60	500	9.15	43.73	35.99	21.05	5.54	11.79	10.13	8.04	4.24	4.82	5.06
170	500	9.89	47.17	39.14	20.35	5.35	10.28	7.65	6.37	5.11	3.92	4.32
159	500	9.94	45.65	37.87	17.98	4.73	14.74	8.91	7.24	3.65	3.27	3.64
23	500	10.05	44.42	36.85	16.43	4.32	11.87	8.42	6.77	3.97	3.66	4.48
24	500	10.37	45.55	37.55	17.92	4.72	10.59	8.74	7.12	4.76	3.90	4.53
164	500	11.17	44.64	37.60	16.93	4.46	8.40	6.32	5.56	3.84	3.35	4.29
40	500	11.23	45.54	37.06	18.94	4.98	13.81	10.48	7.68	3.36	3.47	4.14
34	500	11.79	47.07	39.05	21.65	5.70	8.58	8.78	8.79	7.73	8.20	8.22
15	500	12.01	44.38	35.89	18.00	4.74	12.44	8.49	7.25	5.75	5.47	5.90
100	500	12.58	44.33	36.69	16.19	4.26	13.16	7.32	5.89	3.68	3.77	3.08
158	500	12.82	46.23	36.72	17.06	4.49	11.14	8.02	6.07	2.93	3.87	4.11
2	500	12.82	43.94	36.40	16.75	4.41	12.35	8.44	7.13	6.01	4.59	4.60
157	500	13.83	42.43	35.19	12.38	3.26	9.80	6.14	4.75	2.75	2.41	2.53
22	500	14.19	41.99	33.93	4.59	1.21	10.39	6.21	4.05	0.30	0.30	0.41
162	500	14.86	43.93	35.62	14.44	3.80	10.63	7.45	6.02	4.23	3.64	3.70
1	500	15.16	43.47	34.72	16.89	4.44	11.70	9.19	7.06	3.03	3.08	3.66
165	500	15.29	44.61	35.68	15.75	4.14	10.66	6.80	5.56	3.52	4.09	3.32
163	500	15.39	43.22	35.22	5.04	1.33	10.39	7.18	4.43	0.29	0.33	0.38
110	500	15.71	39.99	31.55	12.30	3.24	8.75	5.60	4.62	2.01	2.80	2.70
42	550	15.85	40.51	32.54	5.12	1.19	8.29	5.35	3.46	0.63	1.01	0.84
130	500	17.18	42.48	32.43	9.37	2.47	12.71	9.24	7.77	6.25	6.02	4.86
174	550	17.40	40.38	31.56	4.87	1.13	8.52	5.79	3.84	0.23	0.23	0.24
13	500	18.63	41.70	33.59	10.78	2.84	10.93	5.76	4.59	2.05	2.64	2.15
111	500	19.34	36.81	28.38	4.10	1.08	10.94	6.63	4.08	0.23	0.21	0.22
67	500	20.11	38.88	30.32	4.51	1.19	8.40	5.69	3.63	0.28	0.24	0.25
68	500	20.36	39.90	30.33	4.81	1.27	9.91	5.69	3.96	0.24	0.24	0.42
97	500	22.55	40.59	32.90	3.83	1.01	N/A	5.02	3.18	0.30	0.26	0.27
172	500	23.34	40.34	32.28	4.54	1.19	8.20	4.45	3.42	0.23	0.22	0.26
70	500	26.03	40.33	30.83	3.94	1.04	8.78	4.63	3.11	0.18	0.19	0.14
62	500	26.39	37.25	34.10	2.41	0.63	4.55	2.53	1.68	0.23	0.23	0.21
61	500	32.68	32.50	28.55	2.21	0.58	4.59	2.25	1.54	0.19	0.18	0.13
63	500	33.65	33.59	29.28	2.31	0.61	4.99	2.64	1.75	0.14	0.17	0.17

N.b. L_0 is the bar length, δ_u is the total displacement at the ultimate force. For the bars in which the failure zone was not captured by the DIC or the reference length moved outside the DIC measuring volume, some values of the ultimate strain were not available.

3.4.3. Influence of gauge length and position on the relationship between ultimate strain versus μ_{max}

As the local axial strain is non-uniform along the corroded bars, the strain computed from different gauge lengths and at different locations varies. The ultimate strains from six different extensometers shown in Fig. 4 are compared in Fig. 14. They are all normalised in respect of the average ultimate strain of uncorroded bars. The ultimate strains calculated from the total elongation of the original tested length 380 or 430 mm, labelled as l_g = 380 mm are also shown in Fig. 14. The normalised ultimate strain shows clear decreasing tendencies with increasing μ_{max}, except for ε_u^{25}. For ε_u^{25}, some points are close to, or even greater than, the strain of uncorroded bars while others are less. This might be due to the fact that the pit length is greater than 25 mm for some bars. In this case, the extensometer can only measure the local yielding level inside the pit, while the strain outside the pit is not captured.

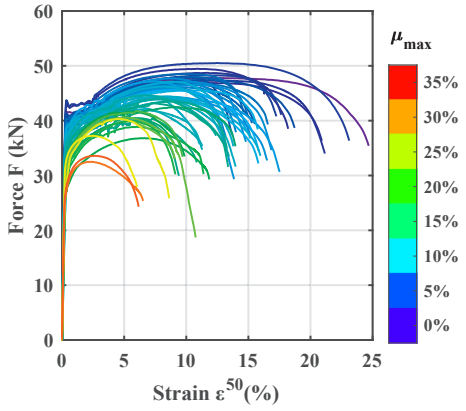

Fig. 7. Force-strain curves of bars with different maximum local corrosion levels.

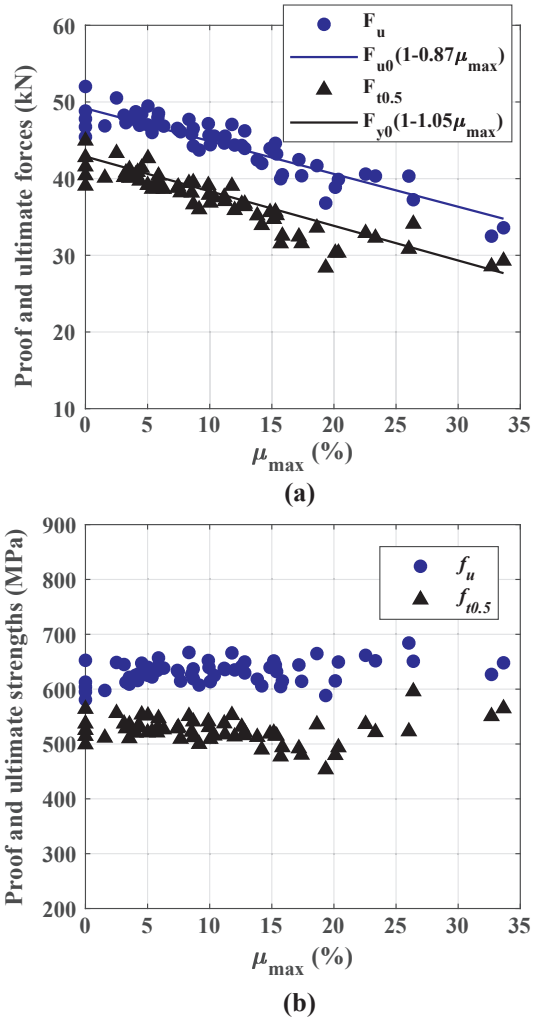

Fig. 8. (a) Proof and ultimate forces versus maximum local corrosion level, with fitting relations; (b) proof and ultimate strengths versus maximum local corrosion level.

For the same bar, increasing the gauge length of the extensometer across the failure zone from 25 mm to 75 mm results in a decrease in ultimate strain. This can be explained by the progressive reduction of the relative contribution of the local strain in the pit to the total deformation over the gauge length, as the gauge length increases. Accordingly, the ultimate strain based on the total elongation of the tested length ε_u^{380} is further reduced, as can be seen in Fig. 14.

In contrast to this, the ultimate strain from the extensometers outside the failure zone is not influenced by the gauge length (5, 10 and 25 mm). Moreover, most values of $\varepsilon_u^{5\_out}$, $\varepsilon_u^{10\_out}$, $\varepsilon_u^{25\_out}$ are lower than ε_u^{380}, as the large local strain inside the pit contributes to an increase in the value of ε_u^{380}. In a few bars, however, the values of $\varepsilon_u^{5\_out}$, $\varepsilon_u^{10\_out}$, $\varepsilon_u^{25\_out}$ are greater. This can be explained by the position of the extensometers in them, which were located outside the failure zone but remained within the corrosion pit zone, where strain localisation still occurred.

Moreover, it is interesting to note that a sudden, greater loss of ultimate strain ($\varepsilon_u^{5\_out}$, $\varepsilon_u^{10\_out}$, $\varepsilon_u^{25\_out}$ and ε_u^{380}) occurred at a corrosion level between 13 and 15%. Quantitatively speaking, the ultimate strain values measured outside the pit for higher corrosion levels dropped below the yield strain of uncorroded bars, $\varepsilon_{y0} = 0.27\%$. Conversely, the values of ε_u^{380} were still greater than the yield strain, even at greater corrosion levels, due to the contribution of strain localisation at the pit. From Fig. 9e–g, it can also be observed that the local strain outside the pit is below the yield strain for bars with higher corrosion levels. It may thus be inferred that a critical local corrosion level exists and that it prevents the yield penetration from developing outside the corrosion pit.

4. Discussion

4.1. Ultimate strain over any gauge length of corroded bars

When analysing the structural behaviour of reinforced concrete analytically or numerically in engineering practice, the reinforcing bars are usually treated as a homogeneous material. For corroded rebars, since the strain capacity along the bar length becomes non-uniform due to the strain localisation, the defined ultimate strain of corroded rebars should be able to represent their strain capacity in an appropriate structural scale length. However, it is not obvious what gauge length should be used to determine the strain capacity of corroded bars. To be on the safe side, long gauge lengths should ideally be selected, although further study on this aspect is still required. This section has attempted to derive the ultimate strain of a corroded bar as a function of gauge length and corrosion level.

4.1.1. Lower-bound solution of the ultimate strain of corroded bars with single localised pit

This section proposes an analytical model for calculating the ultimate strain of a corroded bar, for cases when the gauge length, l_g, is greater than the pit length, l_p, as presented schematically in Fig. 15. According to the results from the DIC measurement described above, the distribution of local strain in a pit was found to be strongly dependent on pit morphology, whilst being almost constant outside the pit, except for the rib effect. Therefore, the ultimate strain of a corroded bar may be obtained from the following equation:

$$\varepsilon_u^{l_g} = \frac{\int_0^{l_g} \varepsilon_u(x)dx}{l_g} = \frac{\int_0^{l_p} \varepsilon_u(x)dx + (l_g - l_p)\varepsilon_u^{out}}{l_g} \quad (4)$$

where $\varepsilon_u^{l_g}$ is the ultimate strain over the gauge length, l_g, $\varepsilon_u(x)$ is the local strain at ultimate strain (which is dependent on the pit morphology) and ε_u^{out} is the ultimate strain outside the pit, over any gauge length greater than one rib spacing.

To express the ultimate strain outside the pit ε_u^{out}, the ultimate stress outside the pit σ_u^{out} was first described. The local bending effect in the pit was considered negligible, so a uniaxial force equilibrium was established. Furthermore, the ultimate strength was assumed to be unaffected by corrosion, as only a slight increase was observed at higher corrosion levels, as presented in Section 3.3. When the stress in the minimum cross-section reaches the ultimate strength f_{u0}, the stress

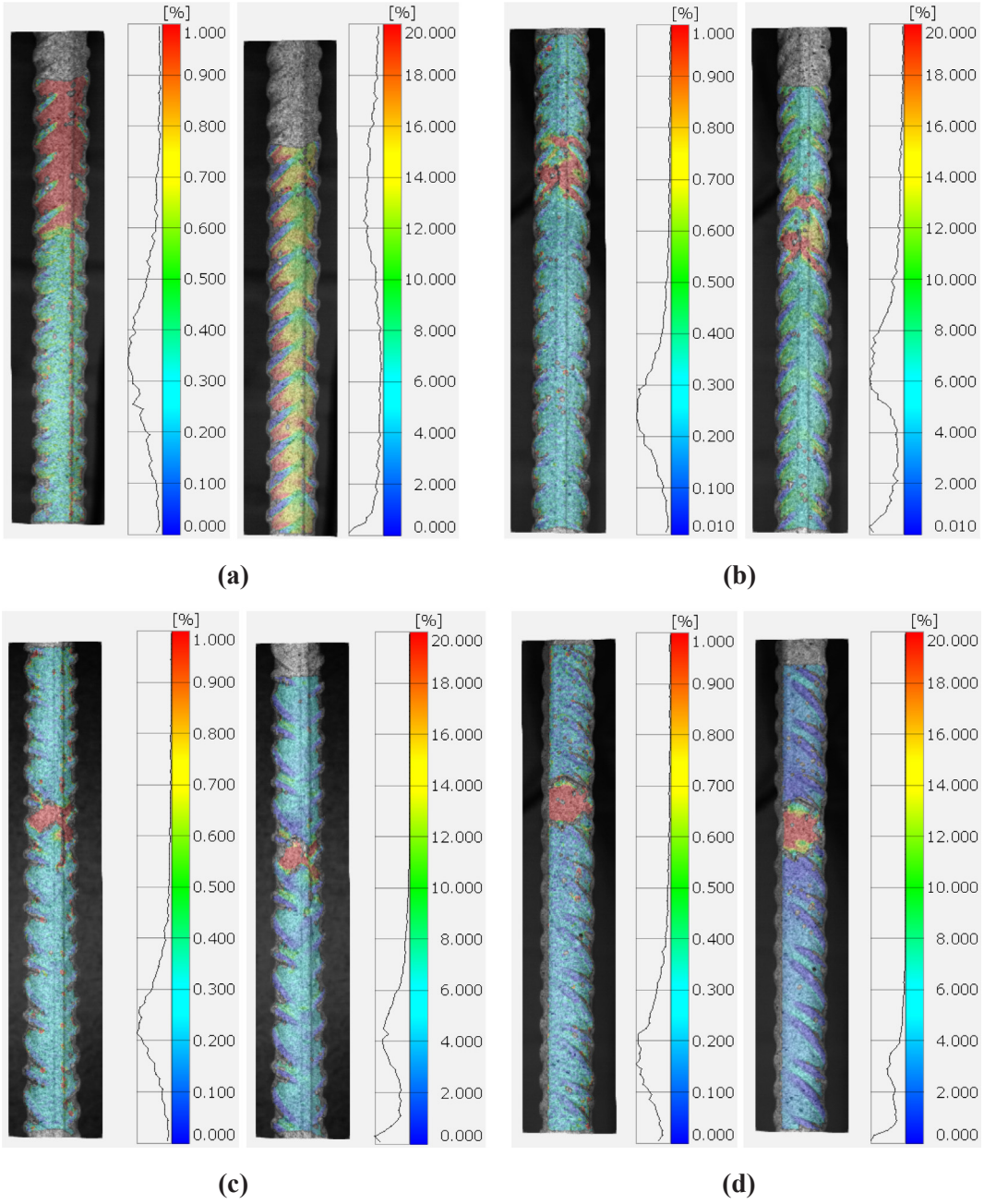

Fig. 9. Local axial strain field at $\varepsilon_{t0.5}$ and ε_u for different corrosion levels: (a)μ_{max} = 0% (b)μ_{max} = 5.4%; (c) μ_{max} = 11.2%; (d) μ_{max} = 15.7% (e); μ_{max} = 20.4%; (f)μ_{max} = 26.0%; (g)μ_{max} = 32.7%.

outside the pit can be calculated from:

$$\sigma_u^{out} A_0 = f_{u0} A_{min} \tag{5}$$

As the minimum cross-sectional area A_{min} is related to the maximum local corrosion level through Eq. (1), the stress outside the pit can be expressed as a function of the maximum local corrosion level:

$$\sigma_u^{out} = f_{u0}(1 - \mu_{max}) \tag{6}$$

The stress-strain relationship of the steel outside the pit follows the constitutive law of the uncorroded steel. However, the stress and strain state cannot reach the ultimate state of uncorroded steel, due to premature failure in the pit. The following formula was adopted for the constitutive law of uncorroded steel. It incorporates a linear elastic part, yield plateau and strain-hardening curve described by a power function [28]:

$$\sigma = \begin{cases} E_0 \varepsilon, & \varepsilon < \varepsilon_{y0} \\ f_{y0}, & \varepsilon_{y0} \le \varepsilon \le \varepsilon_{sh0} \\ f_{u0} - (f_{u0} - f_{y0})\left(\frac{\varepsilon_{u0} - \varepsilon}{\varepsilon_{u0} - \varepsilon_{sh0}}\right)^P, & \varepsilon_{sh0} < \varepsilon \le \varepsilon_{u0} \end{cases} \tag{7}$$

where E_0 is Young's modulus, equal to $\frac{f_{y0}}{\varepsilon_{y0}}$, and P is the strain-hardening power, as defined in Eq. (8) [28]:

$$P = E_{sh0} \frac{\varepsilon_{u0} - \varepsilon_{sh0}}{f_{u0} - f_{y0}} \tag{8}$$

where E_{sh0} is the tangent slope at the onset of strain-hardening, ε_{sh0}, also referred to as strain-hardening modulus. From the experimental results of five uncorroded bars, the strain-hardening modulus was about $0.15E_0$. Fig. 16a shows the experimental stress-strain curves of these five uncorroded bars and the theoretical constitutive law, as described by

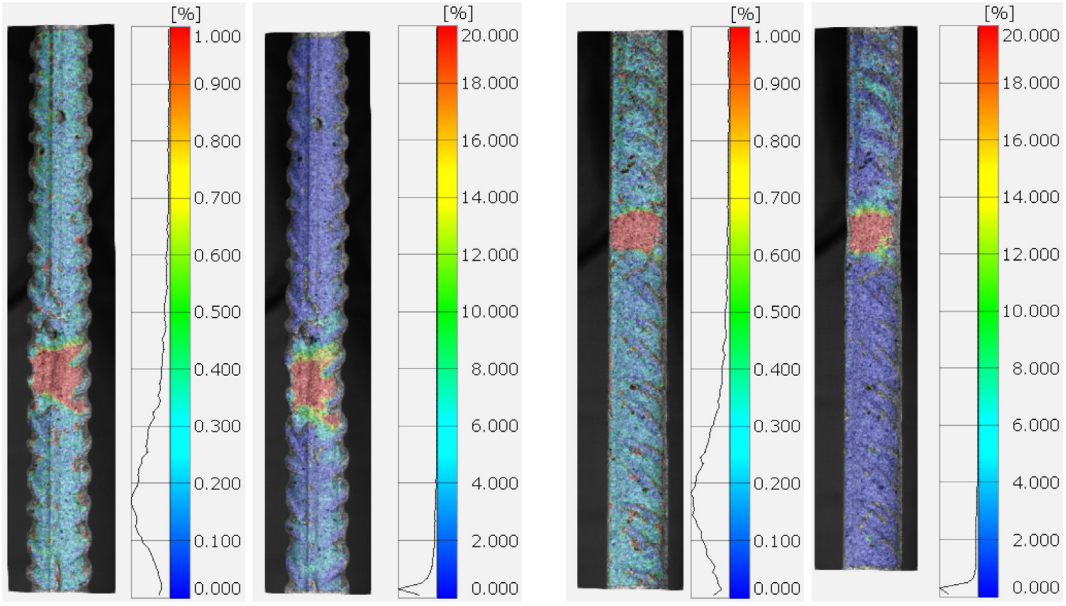

(e) (f)

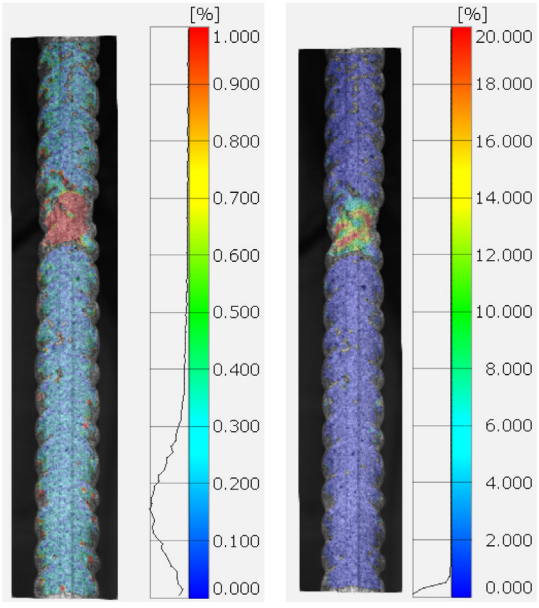

(g)

Fig. 9. (*continued*)

Eq. (7).

From Eq. (7), the strain is expressed in terms of the stress, as in Eq. (9):

$$\varepsilon = \begin{cases} \frac{\sigma}{E_0}, & \sigma < f_{y0} \\ \in [\varepsilon_{y0}, \varepsilon_{sh0}], & \sigma = f_{y0} \\ \varepsilon_{u0} - (\varepsilon_{u0} - \varepsilon_{sh0})\left(\frac{f_{u0} - \sigma}{f_{u0} - f_{y0}}\right)^P, & f_{y0} < \sigma \le f_{u0} \end{cases} \tag{9}$$

Replacing the stress σ in Eq. (9) by σ_u^{out} in Eq. (6), the following relationship between the ultimate strain outside the pit and maximum local corrosion level can be expressed:

$$\varepsilon_u^{out} = \begin{cases} \varepsilon_{u0} - (\varepsilon_{u0} - \varepsilon_{sh0})\left(\frac{f_{u0}}{f_{u0} - f_{y0}}\mu_{max}\right)^P, & \mu_{max} < \mu_{crit} or f_{y0} < \sigma_u^{out} \le f_{u0} \\ \in [\varepsilon_{y0}, \varepsilon_{sh0}], & \mu_{max} = \mu_{crit} or \sigma_u^{out} = f_{y0} \\ \frac{f_{u0}\varepsilon_{y0}}{f_{y0}}(1 - \mu_{max}), & \mu_{max} > \mu_{crit} or \sigma_u^{out} < f_{y0} \end{cases} \tag{10}$$

where μ_{crit} represents the critical local corrosion level above which the bar outside the pit would not yield upon failure within the pit, expressed as follows:

$$\mu_{crit} = 1 - \frac{f_{y0}}{f_{u0}} \tag{11}$$

From the values of f_{y0} and f_{u0} of the bars in this study, the critical local corrosion level μ_{crit} is calculated as 13.3%.

It is interesting to note that the decreasing trend in ultimate strain

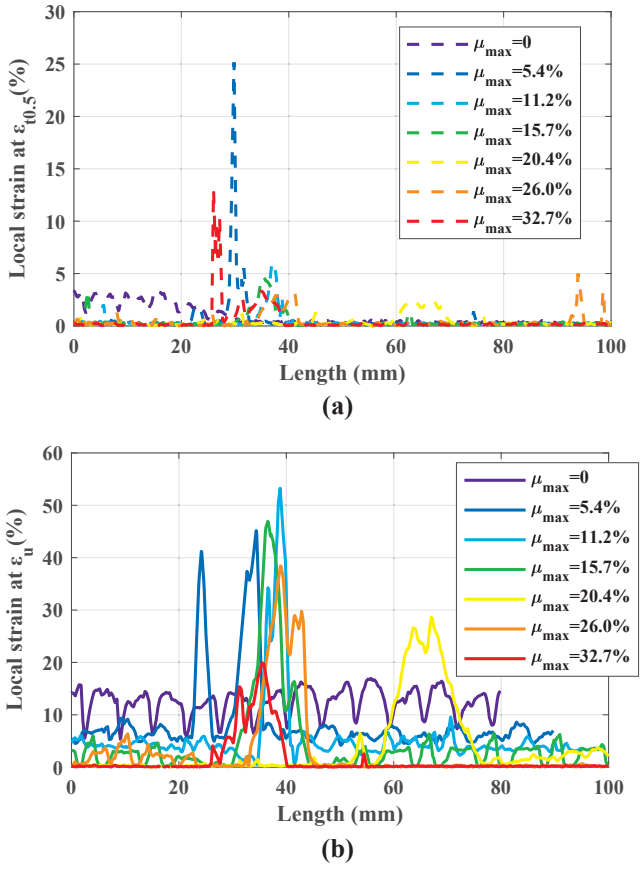

Fig. 10. (a) Local axial strain distribution at $\varepsilon_{t0.5}$; (b) local axial strain distribution at ε_u.

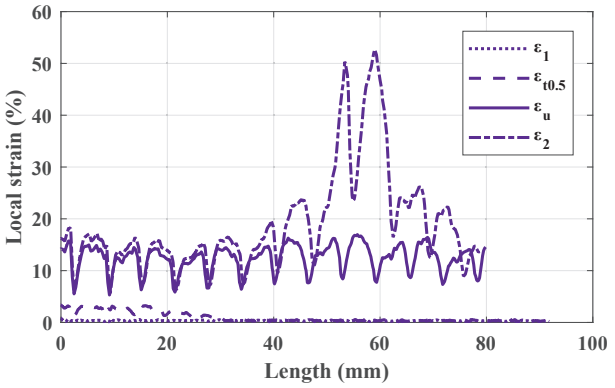

Fig. 11. Local axial strain distribution for an uncorroded bar at four different loading stages: ε_1 ($< \varepsilon_{t0.5}$), $\varepsilon_{t0.5}$, ε_u, ε_2($> \varepsilon_u$).

outside the pit with increasing maximum local corrosion level follows exactly the full constitutive law of uncorroded steel, with the stress replaced by $f_{u0}(1-\mu_{max})$, as shown in Fig. 16b. Further, the comparison between the theoretical results of ε_u^{out} from Eq. (10) and experimental results of $\varepsilon_u^{25\_out}$ in Fig. 16b shows good agreement on the location of the critical local corrosion level, where a sudden drop in ultimate strain was observed for the experimental data $\varepsilon_u^{25\_out}$. However, the experimental data generally shows greater strain values than the analytical solution of ε_u^{out}. This may be because the experimental specimens did not have the idealised single pit shown in Fig. 15. Other minor pits also existed in some bars, which also led to some strain localisation outside the failure zone. Also, in some bars, the 25 mm extensometer outside the failure zone was actually located across part of the corrosion region, due to the

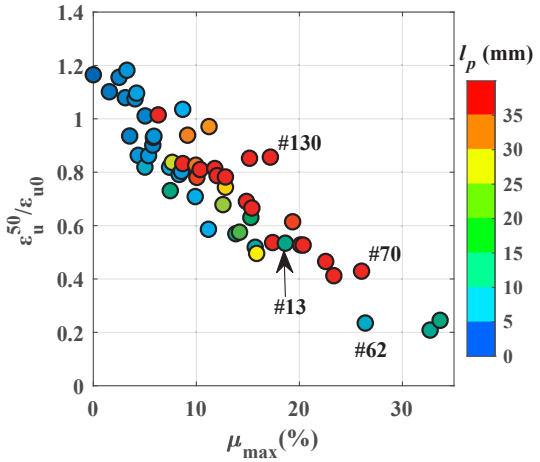

Fig. 12. Normalised ultimate strain ε_u^{50} versus maximum local corrosion level.

DIC's limitations in capturing volume.

The strain inside the pit is much more complex as it is non-uniform and dependent on both the maximum local corrosion level and pit morphology. However, the ultimate strain outside the pit, ε_u^{out} in Eq. (10) can be regarded as a lower-bound solution of Eq. (4) when $l_g \gg l_p$, as it is on the safe side to neglect the strain inside the pit. Consequently, a lower bound for the ultimate strain of a corroded rebar can be estimated directly from the constitutive law for uncorroded rebars, if the maximum local corrosion level is known. This may prove very valuable in engineering practice.

To determine a more accurate ultimate strain value, including the contribution of local strain within the pit, the relationship between local strain distribution and pit morphology needs to be unravelled. Nevertheless, a semi-analytical model is proposed below, as a feasible means of calculating a more accurate ultimate strain value over any gauge length. This is based on the proposed analytical method, using the empirical relationships between ultimate strain and maximum local corrosion level shown in the experimental data from the present study.

4.1.2. Semi-analytical model for rebars in this study

Although the first part of the numerator in Eq. (4) $\int_0^{l_p} \varepsilon_u(x)dx$ (the total strain within the pit) is not known explicitly for each corrosion level, the strain measured from the extensometer across the failure zone included this part. From the experimental results in this study, an empirical relationship was obtained for the ultimate strain over a 50 mm extensometer ε_u^{50}, as a function of the maximum local corrosion level. For the second part of the numerator in Eq. (4), the strain outside the pit, ε_u^{out}, can be described by Eq. (10), or related empirically to the maximum local corrosion level from the experimental results. As discussed in the previous section, Eq. (10) gives lower values than the experimental data. Therefore, an empirical relationship of $\varepsilon_u^{25\_out}$ versus the maximum local corrosion level from the experimental results was used.

With empirical relationships describing ε_u^{50} and $\varepsilon_u^{25\_out}$ as functions of the maximum local corrosion level, the ultimate strain over any gauge length greater than 50 mm can be calculated as:

$$\varepsilon_u^{l_g} = \frac{(50\text{mm})\varepsilon_u^{50} + (l_g - 50mm)\varepsilon_u^{25\_out}}{l_g} \tag{12}$$

An exponential fitting was conducted for ε_u^{50} versus maximum local corrosion level. This fitting has been commonly used in previous studies [5,6,10,11]. A piecewise relationship was used for the relationship between $\varepsilon_u^{25\_out}$ and maximum local corrosion level, as the ultimate strain dropped suddenly at the critical local corrosion level. Using an exponential formula (below the critical local corrosion level) and a

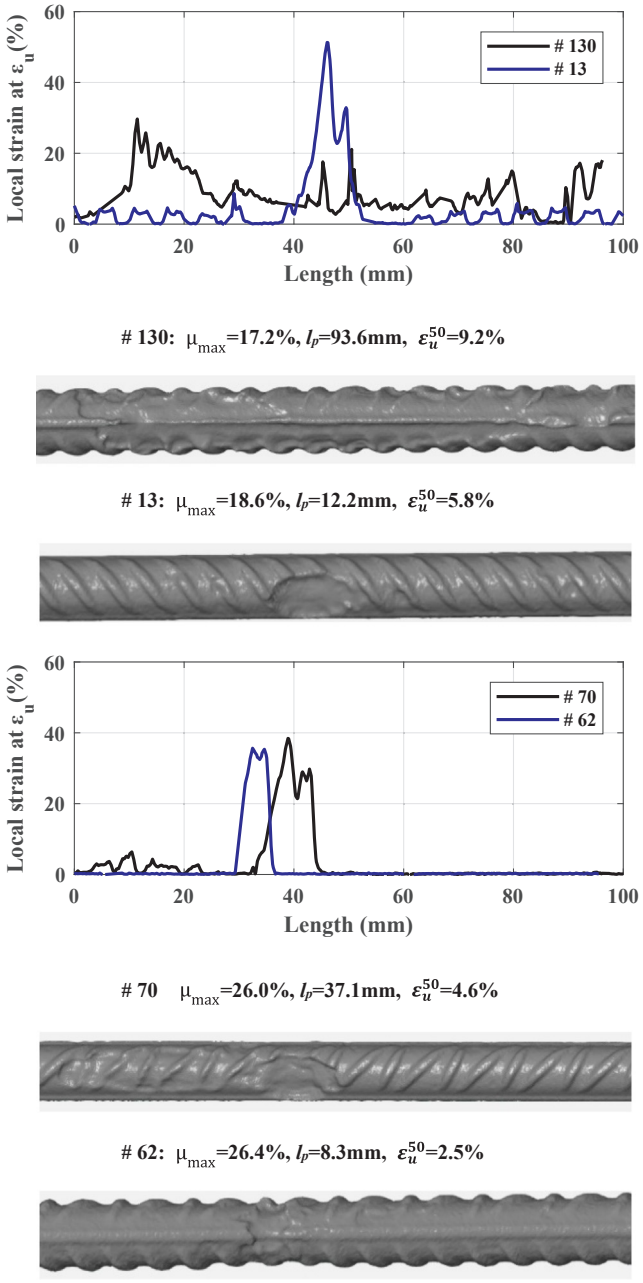

Fig. 13. Comparing local strain distribution under similar maximum local corrosion levels but with significantly different pit lengths.

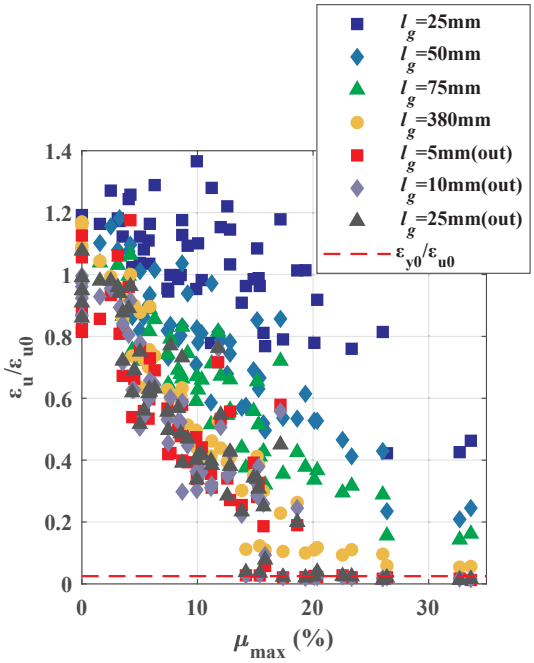

Fig. 14. Normalised ultimate strain from different extensometers versus maximum local corrosion level.

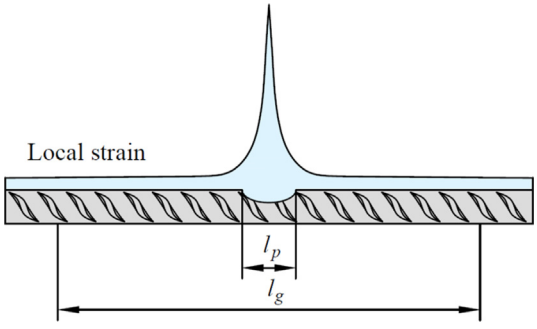

Fig. 15. Schematic diagram showing the bar with pit length l_p.

linear decreasing line (above the critical local corrosion level), the experimental results were well fitted, see Fig. 17a. Theoretically, the exponential curve passes the point (0,1) which represents the average ultimate strain of tested uncorroded bars. Moreover, the second branch for $\varepsilon_u^{25\_out}$ ends at the point (1,0), representing zero strain capacity when the maximum local corrosion level approaches 100%. The empirical relationships for ε_u^{50} and $\varepsilon_u^{25\_out}$ are given in Eqs. (13) and (14):

$$\varepsilon_u^{50} = \varepsilon_{u0} e^{-2.78\mu_{max}} \tag{13}$$

$$\varepsilon_u^{25\_out} = \begin{cases} \varepsilon_{u0} e^{-8.38\mu_{max}}, & \mu_{max} < \mu_{crit} \\ \varepsilon_{u0}(0.0262)(1-\mu_{max}), & \mu_{max} \geq \mu_{crit} \end{cases} \tag{14}$$

The experimental results and fitting relationships are shown in Fig. 17a, with the semi-analytical results of ε_u^{lg} for l_g equal to 100, 200, 300, 400 and 500 mm obtained from Eqs. (12)–(14). For a given maximum local corrosion level, as the gauge length increases, the ultimate strain decreases and tends to approach the value of $\varepsilon_u^{25\_out}$. Taking the gauge lengths as 75 mm and 380 mm, the semi-analytical results compare well with the experimental results of ε_u^{75} and ε_u^{380}, as shown in Fig. 17b. As a result, the semi-analytical model can be used to calculate the ultimate strain over any gauge length greater than 50 mm for bars which have localised pitting corrosion and material properties similar to the bars in this study.

4.2. Comparison of the ultimate strain with the literature

The present experimental data was compared to the results of three previous studies which also measured the maximum local corrosion level of the bars. From Fig. 18, the first noteworthy observation is the large range of results obtained across the different studies. As described in Section 3.4.3, the reported strain values depend on the gauge length used, so the comparison has been made under conditions that are as similar as possible.

A study was reviewed in which the total tested length of the bars (203 mm) had been used to evaluate the ultimate strain (cf. [6]). The results were then compared to those from this study, in which the total elongation had also been measured. This comparison revealed that, for a similar corrosion level, the loss of ultimate strain in the present study was much greater than in [6]. This may be explained by the different corrosion morphologies of the bars in each study. The bars in [6] were

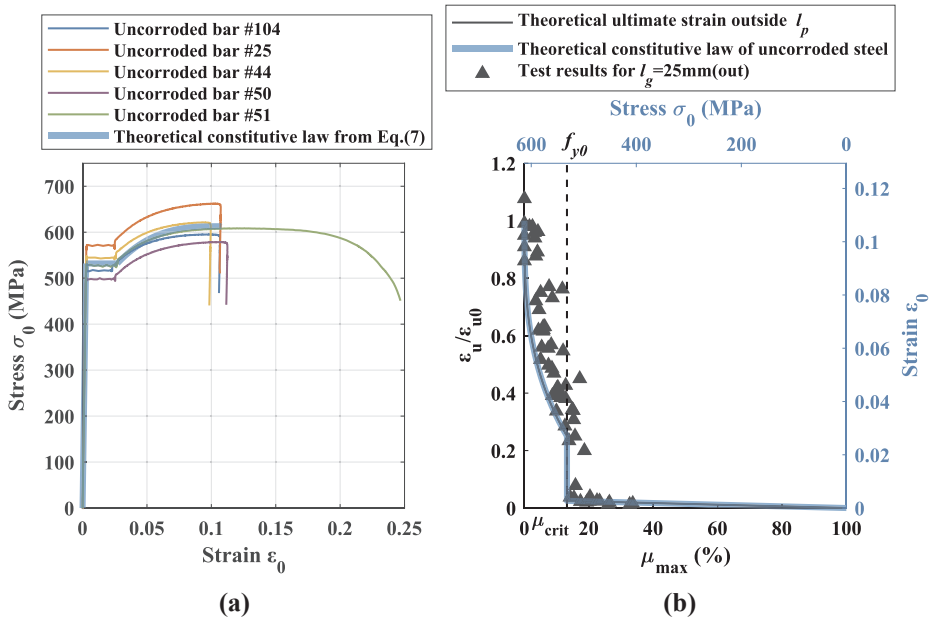

Fig. 16. (a) Stress-strain curves of uncorroded bars and theoretical constitutive law (n.b. the strain in four bars was unloaded because their failure zones were not captured in the DIC); (b) comparison of the theoretical relationship of ε_u^{out}-μ_{max} and experimental results.

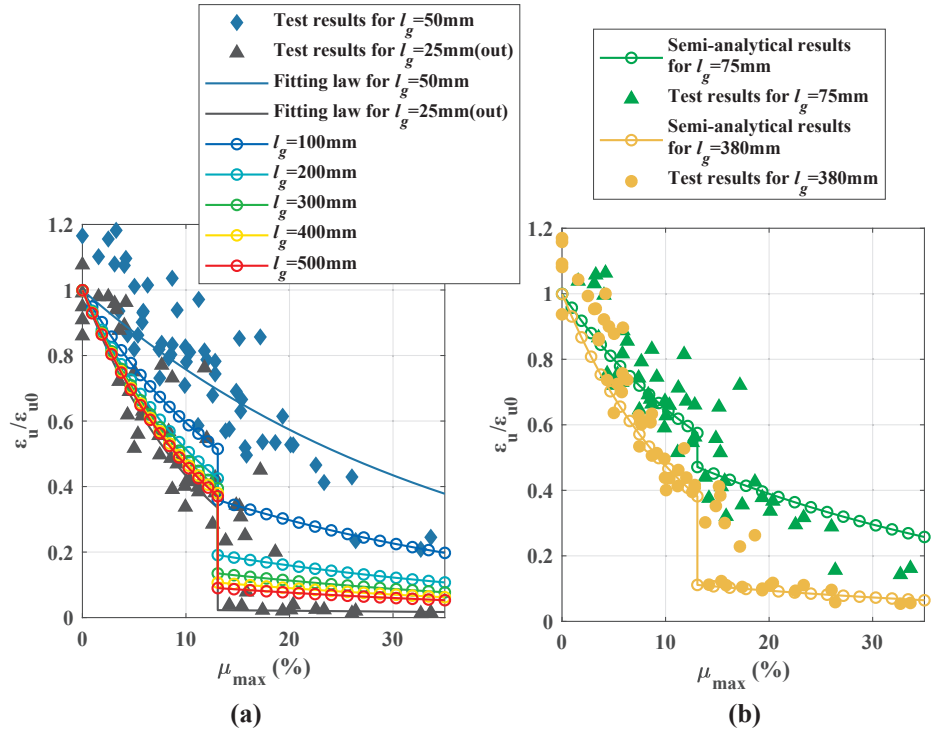

Fig. 17. (a) Ultimate strain for l_g = 50 mm and l_g = 25 mm(out) from experiments and fitting laws; ultimate strain at different gauge lengths obtained from the semi-analytical model; (b) comparison of the ultimate strain obtained from the semi-analytical model and experiments.

corroded along the whole bar surface under impressed current, as opposed to the localised pitting corrosion seen in this study. This indicates that localised pitting corrosion impacts the ductility of corroded bars more adversely than extensive pitting corrosion.

Comparing the results of [13,14], in which short extensometer gauge lengths were adopted (60 mm and 50 mm; similar to the 50 mm extensometer used in this study), again, it may be seen that, for a similar corrosion level, most values in [13,14] are greater than those in the present study. The bars in [13,14] were naturally corroded in real structures. Extensive pitting corrosion along the whole bar surface was observed according to the 3D-scanning results reported in [13,14]. As a result, the bar surfaces in [13,14] presented conspicuous corrosion over the entire length of the extensometer gauge, whereas most of the bars in the present study featured pit lengths shorter than the 50 mm gauge length, as shown in Table 1. Consequently, strain localisation most likely did not occur to the same extent in the bars with extensive pitting corrosion and thus greater ultimate strains were obtained than in this study.

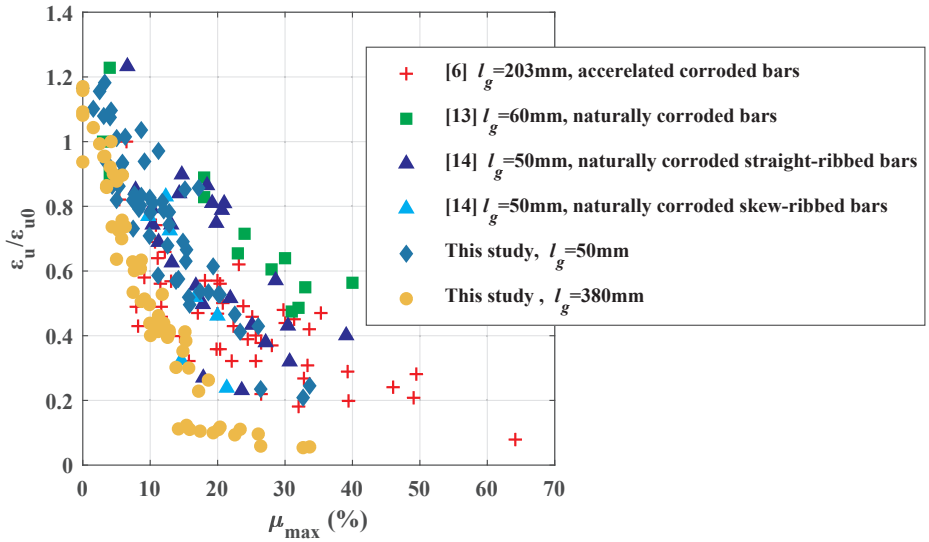

Fig. 18. Ultimate strain versus maximum local corrosion level from different studies.

4.3. Time-dependent assessment of the strain capacity

The corrosion morphology of rebars in real structures is commonly classified as general corrosion induced by concrete carbonation, or pitting corrosion induced by chlorides. For chloride-induced corrosion, the corrosion morphology evolves during the corrosion propagation period. At an early stage, localised pitting corrosion is more likely to initiate near pre-existing cracks, as observed in this study. However, as corrosion-induced cracks propagate longitudinally in rebars, chlorides, oxygen and moisture may penetrate through them, thus promoting broader development of pitting corrosion along the bar length. This argument has also been manifested in [29], in which the study authors compared the corrosion morphology and corrosion-induced cracks of RC beams at different exposure times.

Since the strain capacity of corroded reinforcement bars is significantly affected by corrosion morphology, the time-varying nature of corrosion morphology must therefore be borne in mind when making an assessment. A hypothesis is proposed to illustrate the time-dependent strain capacity at three different corrosion stages in which distinct corrosion patterns are dominant, see Fig. 19. In stage I, corrosion pits are only formed locally; the majority of bars in this study exhibit the corrosion morphology of this stage. The strain capacity decreases rapidly with increasing maximum local corrosion level. In stage II, pits grow along the bar as corrosion-induced cracks develop; a few bars in this study can be classified to this stage. As discussed in Section 3.4.2, longer pits most likely have greater strain capacity than shorter ones of similar maximum local corrosion level. It is therefore feasible that the strain capacity may be partially recovered in this stage. In stage III, when the corrosion-induced cracks extend and connect throughout the whole beam surface, corrosion eventually spreads over the whole rebar surface. The corrosion morphology in this stage is commonly seen in rebars taken from the real structures that have been corroded for decades, as in [13,14]. The comparison of the ultimate strain with the results from the literature [13,14] in Section 4.2 has shown that the degradation of strain capacity in naturally corroded bars with increasing maximum local corrosion level is slower compared to the bars in this study. Consequently, a more gentle slope is expected for the decreasing trend in strain capacity at this stage.

Finally, a naturally corroded rebar retrieved from the edge beam of a real bridge (the Stallbacka Bridge) after 35 years in service [14], was also examined using DIC. The local strain distribution of the naturally corroded rebar was compared to that of a bar with similar maximum local corrosion level and the longest pit length corroded in the laboratory of this study (bar #130), as shown in Fig. 20. Both bars were corroded along the entire length of the DIC capture volume. Large local strains were observed along the whole bar; however, the distribution of the local strain in the naturally corroded bar had more peaks, due to its more irregular corrosion pattern. The ultimate strain for the two bars (based on a 50 mm gauge length) is close. However, the corrosion level (as determined by the total weight loss, μ_{weight}) of the bar in this study was much lower than that of the naturally corroded bar, since the latter was severely corroded across its entire surface. As a result, with increasing corrosion time, although the total steel loss increases, the strain capacity may not necessarily decrease as it depends largely on the corrosion morphology. To predict the time-dependent strain capacity of corroded rebars requires further studies on the evolution of corrosion morphology with concrete cracking and corrosion time.

5. Conclusions

This paper has studied the tensile behaviour of reinforcement bars exhibiting localised pitting corrosion. The non-uniform local strain distribution along the bar length was captured during tensile testing, using the DIC technique. This revealed that the measured ultimate strain was dependent on the extensometer gauge length for a given corrosion pit. The strain localisation in the corrosion pit led to premature failure, whereupon the strain outside the pit could not adequately develop. A lower bound for the ultimate strain in corroded bars with a single localised pit was given as the ultimate strain that can be reached outside the pit. In summary, the following conclusions were

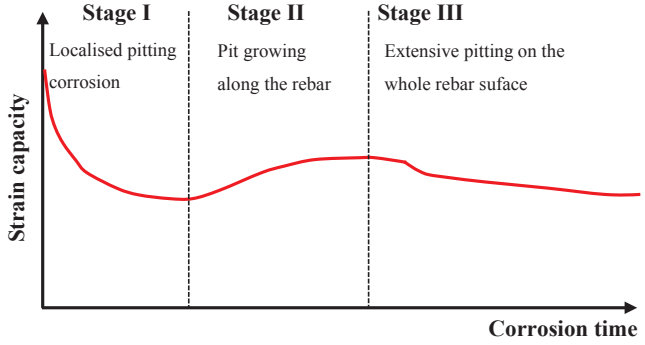

Fig. 19. Evolution of the strain capacity of corroded rebars as the pit morphology evolves with time.

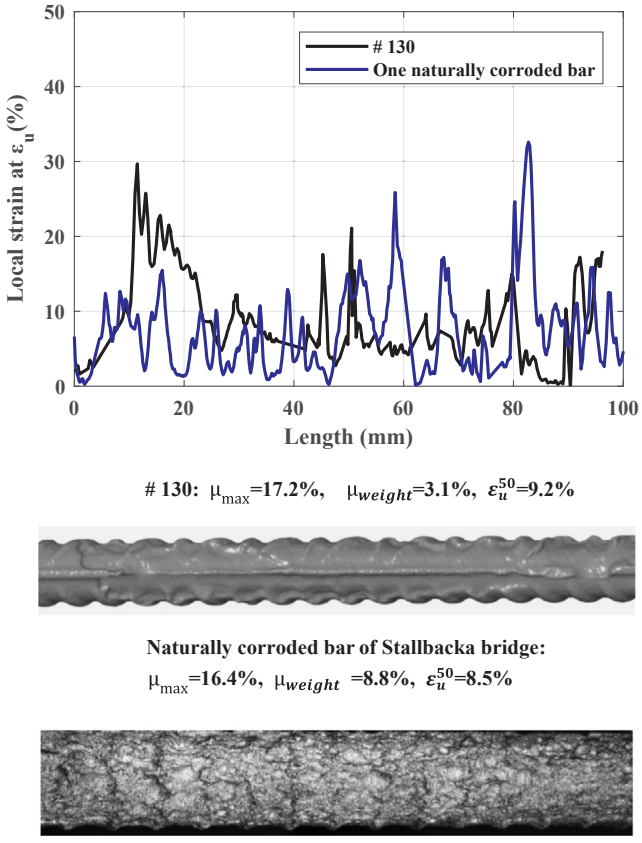

Fig. 20. Comparison of the local strain distribution of the bar with the greatest pit length in this study and a naturally corroded rebar in [14].

drawn from this study:

(1) The shape of the force-strain curve of steel bars was strongly influenced by corrosion. With increasing corrosion level, the force-strain curves displayed earlier yielding, with the yielding plateau disappearing progressively. The proof and ultimate forces decreased linearly with the maximum local corrosion level. However, the proof and ultimate strengths that were based on the minimum remaining cross-sectional area remained nearly constant as the corrosion level increased. There was a slight ascending trend at higher corrosion levels.

(2) The measured ultimate strain of corroded bars depends strongly on gauge length. Caution is therefore advised if experimental results or empirical relationships relating to ultimate strain will be used to assess corroded structures, as few previous studies have covered this.

(3) The ultimate strain outside the corrosion pit reduced significantly as the maximum local corrosion level increased. Moreover, a sudden great loss was observed at a critical local corrosion level. When this was exceeded, the bar outside the pit did not yield. It was shown that the critical local corrosion level is 1 minus the ratio between yield strength and ultimate strength. For the rebars in this study, the value was 13.3%.

(4) A simple analytical model giving a lower-bound solution for ultimate strain was proposed. This was expressed as a function of the mechanical parameters of uncorroded steel and maximum local corrosion level. It compared well with the experimental results and may prove valuable when used in engineering practice.

(5) The empirical relationships were determined of the ultimate strain to the maximum local corrosion level for results from a 50 mm extensometer across the failure zone and a 25 mm extensometer outside it. Based on them, a semi-analytical model was formulated to calculate the ultimate strain over any gauge length exceeding 50 mm. A good comparison was obtained, between the calculated ultimate strain across a long gauge and the experimental results. The choice of the most appropriate gauge length to describe the strain capacity of corroded rebars in concrete structures is a question that requires further study. However, to be on the safe side, a long gauge length should be used.

(6) At similar maximum local corrosion levels, bars with much longer pit length in this study displayed a greater ultimate strain than bars with shorter pit length. Moreover, via comparison with the literature, localised pitting corrosion was found to reduce strain capacity more than extensive pitting corrosion.

(7) As corrosion morphology progresses from localised pitting corrosion (during early corrosion) to extensive pitting corrosion as corrosion-induced cracks propagate, the strain capacity of corroded rebars may initially decrease more rapidly. Thereafter, it may decrease slowly and even gradually increase as the corrosion time progresses. For this reason, it is important to quantify the corrosion morphology and relate it to the strain capacity of corroded bars.

CRediT authorship contribution statement

E. Chen: Conceptualization, Investigation, Methodology, Formal analysis, Visualization, Writing - original draft. **Carlos G. Berrocal:** Conceptualization, Software, Methodology, Writing - review & editing. **Ignasi Fernandez:** Conceptualization, Resources, Writing - review & editing. **Ingemar Löfgren:** Conceptualization, Funding acquisition, Project administration, Writing - review & editing. **Karin Lundgren:** Conceptualization, Formal analysis, Supervision, Writing - review & editing.

Declaration of Competing Interest

The authors declare that they have no known competing financial interests or personal relationships that could have appeared to influence the work reported in this paper.

Acknowledgements

The work reported in this paper has been supported by: the Swedish Transport Administration, under the project grant TRV 2018/36506; the construction industry's organisation for research and development (SBUF) under the project grant 13683; Chalmers University of Technology; Thomas Concrete Group; and Cementa AB (Heidelberg Cement Group).

References

[1] Du Y, Clark L, Chan A. Residual capacity of corroded reinforcing bars. Mag Concr Res 2005;57:135–47.
[2] Cairns J, Plizzari GA, Du Y, Law DW, Franzoni C. Mechanical properties of corrosion-damaged reinforcement. ACI Mater J 2005;102:256.
[3] Zhang W, Song X, Gu X, Li S. Tensile and fatigue behavior of corroded rebars. Constr Build Mater 2012;34:409–17.
[4] Apostolopoulos CA, Demis S, Papadakis VG. Chloride-induced corrosion of steel reinforcement–Mechanical performance and pit depth analysis. Constr Build Mater 2013;38:139–46.
[5] François R, Khan I, Dang VH. Impact of corrosion on mechanical properties of steel embedded in 27-year-old corroded reinforced concrete beams. Mater Struct 2013;46:899–910.
[6] Tang F, Lin Z, Chen G, Yi W. Three-dimensional corrosion pit measurement and statistical mechanical degradation analysis of deformed steel bars subjected to accelerated corrosion. Constr Build Mater 2014;70:104–17.
[7] Moreno E, Cobo A, Palomo G, González MN. Mathematical models to predict the mechanical behavior of reinforcements depending on their degree of corrosion and the diameter of the rebars. Constr Build Mater 2014;61:156–63.
[8] Fernandez I, Bairán JM, Marí AR. Corrosion effects on the mechanical properties of reinforcing steel bars. Fatigue and σ–ε behavior. Constr Build Mater 2015;101:772–83.
[9] Qiao D, Nakamura H, Yamamoto Y, Miura T. Evaluation method of tensile behavior of corroded reinforcing bars considering radius loss. J Adv Concr Technol

2015;13:135–46.
[10] Lu C, Yuan S, Cheng P, Liu R. Mechanical properties of corroded steel bars in pre-cracked concrete suffering from chloride attack. Constr Build Mater 2016;123:649–60.
[11] Zhu W, François R, Poon CS, Dai J-G. Influences of corrosion degree and corrosion morphology on the ductility of steel reinforcement. Constr Build Mater 2017;148:297–306.
[12] Sun X, Kong H, Wang H, Zhang Z. Evaluation of corrosion characteristics and corrosion effects on the mechanical properties of reinforcing steel bars based on three-dimensional scanning. Corros Sci 2018;142:284–94.
[13] Subramanian SJ, Sharma S, Rajagopal R, Pillai RG. Assessment of Stress-Strain Behavior of Corroded Steel Reinforcement Using Digital Image Correlation (DIC). J Test Eval 2018;46:1874–90.
[14] Fernandez I, Berrocal CG. Mechanical properties of 30 year-old naturally corroded steel reinforcing bars. Int J Concr Struct Mater 2019;13:9.
[15] Fernandez I, Bairán JM, Marí AR. Mechanical model to evaluate steel reinforcement corrosion effects on σ–ε and fatigue curves. Experimental calibration and validation. Eng Struct 2016;118:320–33.
[16] Angst U, Elsener B, Jamali A, Adey B. Concrete cover cracking owing to reinforcement corrosion–theoretical considerations and practical experience. Mater Corros 2012;63:1069–77.
[17] Eurocode. 2: design of concrete structures–Part 1-1: general rules and rules for buildings: EN 1992-1-1. European Committee for Standardization; 2004. p. 225.
[18] Berrocal CG, Löfgren I, Lundgren K, Tang L. Corrosion initiation in cracked fibre reinforced concrete: influence of crack width, fibre type and loading conditions. Corros Sci 2015;98:128–39.
[19] Fernandez I, Lundgren K, Zandi K. Evaluation of corrosion level of naturally corroded bars using different cleaning methods, computed tomography, and 3D optical scanning. Mater Struct 2018;51:78.
[20] Tahershamsi M, Fernandez I, Lundgren K, Zandi K. Investigating correlations between crack width, corrosion level and anchorage capacity. Struct Infrastruct Eng 2017;13:1294–307.
[21] MATLAB R2017b. The MathWorks, Inc. Natick, Massachusetts, United States.
[22] Berrocal CG, Löfgren I, Lundgren K. The effect of fibres on steel bar corrosion and flexural behaviour of corroded RC beams. Eng Struct 2018;163:409–25.
[23] ISO. BS EN 6892-1. Metafile Metallic materials-Tensile testing-Part 12016.
[24] Cato A, Raju MR. Mechanical properties of naturally corroded steel bars: Experimental study [Master of Science]. Göteborg, Sweden: Chalmers Univeristy of Technology; 2018.
[25] GOM Correlate Professional; 2018.
[26] Chen E, Berrocal CG, Löfgren I, Lundgren K. Correlation between concrete cracks and corrosion characteristics of steel reinforcement in pre-cracked plain and fibre-reinforced concrete beams. Mater Struct 2020;53:1–22.
[27] Fernandez I, Bairán JM, Marí AR. 3D FEM model development from 3D optical measurement technique applied to corroded steel bars. Constr Build Mater 2016;124:519–32.
[28] Mander JB. Seismic design of bridge piers. Christchurch, New Zealand: University of Canterbury; 1983.
[29] Zhang R, Castel A, François R. The corrosion pattern of reinforcement and its influence on serviceability of reinforced concrete members in chloride environment. Cem Concr Res 2009;39:1077–86.